

Comparative Analysis of ACM and GPWM Controllers in Continuous Input and Output Power Boost PFC Converter

Maheswari Ellappan^{*}, Kavitha Anbukumar^{**}

^{*} Department of EEE, Sri Sairam Institute of Technology, Anna University, Chennai, India
(e-mail:maheseee25@rediffmail.com)

^{**} Department of EEE, Anna University, Chennai, India
(e-mail:akavitha@annauniv.edu)

Abstract: Continuous input and output power converters are extensively used in renewable energy applications. In this paper, firstly the bifurcation analysis is carried out in a new topology of Continuous input and output power boost converter. The reference current is varied to realize the current mode control during the bifurcation analysis. The chaos occurs through quasi periodic bifurcation. The Jacobian matrix is derived to analyze the stability of the converter and it is found that the system loses its stability through quasi periodic bifurcation. Secondly to improve the power factor and to reduce the harmonic component in the input side of the AC source, the active power factor correction (PFC) controllers like Average Current Mode (ACM) controller and General Pulse Width Modulation (GPWM) controller are used. The performances of these two controllers are compared for line and load variation. The multiplier and amplifier circuit is eliminated in the GPWM controller compared to the ACM controller. The simulated results are validated with the experimental results obtained from the designed prototype model of the 40W output power converter.

Keywords: Bifurcation, Chaos, Current control, Continuous input and output (CIO) power Converters, Total harmonic distortion

1. INTRODUCTION

DC and AC motors for industrial and commercial applications suffer from lagging power factor issues. Maintaining high power factor and voltage regulation is indeed a challenge during line and load variations in the DC and AC drives. The active power factor correction controller plays an effective role in overcoming the drawback associated with lagging power factor issues.

In recent years' maximum power utilization is achieved by incorporating continuous input and output power dc to dc converters in tandem with grid connected renewable energy sources. The continuous input and output power converter offers the lowest THD and optimum power factor correction to claim high efficiency at high power level while being designed with high power density. Boost type PFC converters realized as the first stage of the PV and fuel cell applications (Williams, 2013; Nahla et al., 2019) offer unity power factor and better output voltage regulation. In future, these converters can be connected in parallel for DC microgrid applications with continuous input and output power using equal current sharing method (Zhuang et al., 2018; Muamer et al., 2020).

Nonlinear phenomena like bifurcation and chaos (Sajid et al., 2014; Yesoda et al., 2013) occur in power electronic circuits when there is variation in system parameters. Bifurcation helps in identifying the dynamics of interest existing in configuration space. Stability boundaries are realized as a function of parameters controlling the system operation. The

system loses the fundamental operation and enters into the chaotic region through quasi periodic bifurcation when there is variation in system parameters like reference current, load resistance, and input voltage of the converter. The system parameters are adjusted to optimum value while the design confirms a safe operating region with the help of bifurcation analysis (Kavitha et al., 2010; Zhioua et al., 2016; Ruiye et al., 2019). The averaged state space model is used to determine the Eigen value movement from stable state to unstable state, thereby aiding in estimating the stability and dynamic behaviour of the power converters by deriving the Jacobian matrix (Hu et al., 2017; Mei et al., 2016; Hengsi et al., 2011; H.H.C.lu et al., 2003). The integral sliding mode controller is applied in a hybrid power system to get the maximum power across the load side using basic boost converter topology (Masoud et al., 2019).

The two types of instability that occur in CUK power factor correction converter is the fast scale and slow scale instability and it was controlled using the Non linear carrier (NLC) controller. It is similar to switch current control method (Kavitha et al., 2012; Deivasundari et al., 2013). The line current is distorted in the discontinuous operation mode of boost PFC converters (Yang et al., 2016; Xiaotian et al., 2011).

Unlike the dc to dc converter, the boost PFC converters are fed from a rectified dc voltage as the input. To reduce the conduction loss and voltage stress, the bridgeless PFC converters also implemented in the high gain converter circuit (Xiang et al., 2018; Bhim et al., 2019; Yi-Hung Liao., 2020). PFC converters suffer from two nonlinear phenomena

like instability at the line frequency and instability at the switching frequency (Herbert et al., 2003; Orabi et al., 2003; Chu et al., 2009; Faqiang et al., 2010). The performance of the system is highly affected by instability at the line frequency rather than instability at the switching frequency (Mazumder et al., 2001; Aroudi et al., 2008).

Active Power Factor Correction controllers, i.e., Average Current Mode Control (ACM) and General Pulse Width Modulation Controllers (GPWM) are the two different control methods applied in PFC controllers (Zheren et al., 1998). The GPWM method with reduced complex circuits and lesser essential external components deliver fast transient response and excellent input disturbance rejection. These significant features have made the GPWM method is a successful control method for the power factor correction (PFC) converter circuit (Hao et al., 2012).

Based on the literature survey, it is evident that the nonlinear behavior and control is realized only in basic Buck, Boost, Buck-Boost, CUK, ZETA, and SEPIC PFC converters (Giaouris et al., 2012; Weibin et al., 2015; Wei et al., 2011; Tse., 2003). The stability analysis and performance of the SEPIC PFC Converter is compared for ACM and Enhanced NLC controller methods. Both the controllers requires complex external component in input side of the converter (Radha et al., 2020).

The simulation study of Bifurcation behavior in the new topology of CIO power Buck-Boost PFC converter is analyzed using the ACM and NLC controllers. This converter loses its stability through period-doubling bifurcation when the reference current and input voltage values are varied (Maheswari et al., 2016).

In this research article, the new topology of the CIO power boost converter is designed and this converter loses its stability through quasi-periodic bifurcation under current mode control. The CIO Power Boost and Buck-Boost converter give the continuous load current for a wide variation of duty ratio compared to Basic dc to dc converters. The stability of the converter is studied with the movement of Eigen values using the Jacobian matrix. Then the performance behavior in CIO power Boost PFC converter is analyzed using ACM and GPWM controller. When the ACM controller is implemented in both the new topologies of CIO power PFC converters it requires the input voltage sensor, current sensor, and multiplier as well as amplifier circuit. The switch current sensor and current transformer are required in the NLC controller of the CIO power Buck-Boost PFC converter. It makes switch current stress across the device. To overcome these disadvantages of the ACM and NLC controller, the GPWM controller is implemented in Continuous input and output power Boost PFC converter. The FFT analysis, THD and power factor values are compared for two controllers by varying the input voltage and load resistance.

The motivation of the paper is to realize an efficient control method for the Continuous input and output power boost converter to extract maximum power at unity power factor,

with the high power density and reduced distortions without compromising reliability and repeatability of the system.

This paper is organized as follows. Section 2 reviews the operation of the Continuous input and output power boost converter. Section 3 reviews the Bifurcation analysis of the converter. Section 4 presents, PFC with the ACM controller; section 5 reviews the PFC with GPWM controller and comparative analysis; Experimental results are presented in section 6; Conclusion is stated in Section 7.

2. OPERATION OF CIO POWER BOOST CONVERTER

The circuit diagram of continuous input and output (CIO) power boost converter is shown in Fig.1. CIO offers continuous input and load current for a low duty cycle when compared to a normal boost converter. Maximum power is extracted from the renewable energy sources with the CIO converters. The operation of the CIO Boost converter explained based on mode 1 and mode 2 operations.

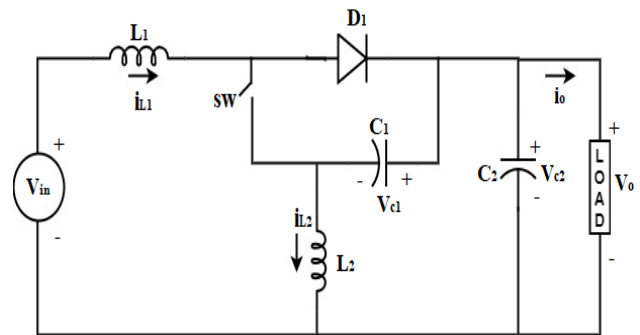


Fig. 1. Circuit Diagram for CIO Power Boost Converter.

2.1 Mode 1 operation

In mode 1 operation when the switch is in ON stage, L_1 gets charged through the input voltage and energy from the inductor L_2 . The capacitor C_1 and inductor L_2 discharges. The capacitor C_2 charges during ON condition.

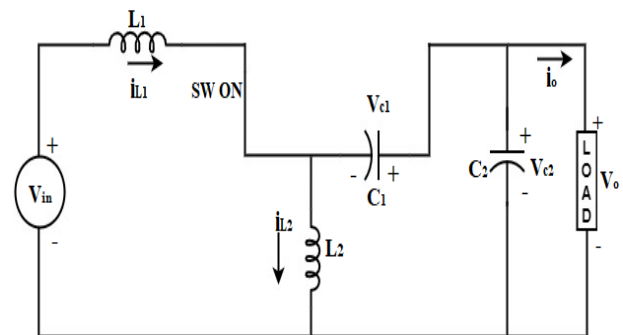


Fig. 2. Circuit Diagram for Mode 1 Operation.

2.2 Mode 2 operation

In mode 2 operation, the switch is in the OFF stage and the diode is in forward biased condition. The capacitor C_1 and inductor L_2 charged through input voltage and energy from the inductor L_1 . The inductor L_1 and capacitor C_2 discharges.

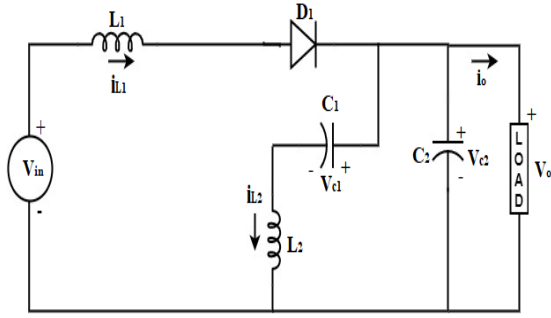


Fig. 3. Circuit Diagram for Mode 2 Operation.

The state equation of the system for mode 1 and mode 2 operations are given as follows. These equations are used to find the stability state of the system.

The state variables are $x_1 = V_{C1}, x_2 = V_{C2}, x_3 = i_{L1}, x_4 = i_{L2}$. V_{C1} is a voltage across the Capacitor C_1 , V_{C2} is a voltage across the Capacitor C_2 , i_{L1} is a current flow through inductor L_1 , i_{L2} is a current flows through inductor L_2 .

$$A_1 = \begin{bmatrix} 0 & 0 & \frac{1}{C_1} & -\frac{1}{C_1} \\ 0 & \frac{1}{RC_2} & -\frac{1}{C_2} & \frac{1}{C_2} \\ \frac{1}{L_1} & -\frac{1}{L_1} & 0 & 0 \\ -\frac{1}{L_2} & \frac{1}{L_2} & 0 & 0 \end{bmatrix} \quad B_1 = \begin{bmatrix} 0 \\ 0 \\ \frac{1}{L_1} \\ 0 \end{bmatrix} \quad (1)$$

$$A_2 = \begin{bmatrix} 0 & 0 & 0 & -\frac{1}{C_1} \\ 0 & \frac{1}{RC_2} & -\frac{1}{C_2} & \frac{1}{C_2} \\ 0 & -\frac{1}{L_1} & 0 & 0 \\ -\frac{1}{L_2} & \frac{1}{L_2} & 0 & 0 \end{bmatrix} \quad B_2 = \begin{bmatrix} 0 \\ 0 \\ \frac{1}{L_1} \\ 0 \end{bmatrix} \quad (2)$$

2.3 Design parameters of the converter

The converter components are designed based on Kirchhoff's voltage and current law equations framed from the mode 1 and mode 2 operations. The inductors and capacitors are designed based on the duty ratio 0.5 with a switching frequency of 25 kHz. The design parameters are shown in Table 1.

Input current ripple $\Delta I = 5\%$, Output voltage ripple $\Delta V_c = 5\%$, Input voltage $V_{in} = 20V$, Output power $P = 40W$.

$$\text{Output voltage } V_o = \frac{V_{in}}{1-d} = 40V \quad (3)$$

$$\text{Output Current } I_o = \frac{P}{V_o} = 1Amps \quad (4)$$

For lossless condition input power is equal to output power.

$$V_{in} * I_{in} = V_o I_o \quad (5)$$

From the equation (3),(4) and (5) the input current I_{in} is equal to 2Amps.

$$\text{Inductance } L_1=L_2 = \frac{V_{in} * d}{f * \Delta I} = 4mH \quad (6)$$

$$\text{Input capacitor } C_1 = \frac{I_o}{f} * \frac{d}{\Delta V_c} = 10\mu F \quad (7)$$

$$\text{Output capacitor } C_2 = \frac{dV_{in}}{8f^2 L_2 \Delta V_c} = 1\mu F \quad (8)$$

Table 1. Design Parameters.

S.NO	Parameters	Specifications
1	Input Voltage (V_{in})	20V
2	Output Power (P)	40W
3	Switching Frequency (f)	25kHz
4	Inductors (L_1 & L_2)	4mH
5	Capacitor C_1	10 μ F
6	Capacitor C_2	1 μ F

3. BIFURCATION ANALYSIS OF THE CONVERTER

The bifurcation analysis is carried out using MATLAB/SIMULINK model by varying the converter reference current using current mode control. The simulation results are explained as follows.

3.1. Variation in i_{ref}

The stability of the converter is analyzed by varying the reference current i_{ref} . The reference current is set and compared with the inductor current as shown in Fig.4. The switch is turned off when both the currents become equal and turned on according to the clock. The stable operation is obtained when the reference current is 2.03A.

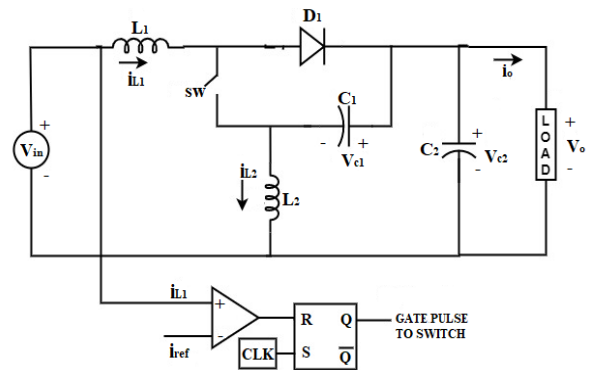


Fig. 4. Circuit Diagram of Current Mode Control.

The converter loses its stability and it enters into the chaotic region through quasi periodic bifurcation when the reference current varied from 2.15A to 3A. Fig.5, Fig.6, and Fig.7 show the simulated fundamental, quasi periodic and chaos waveforms for output voltage, Inductor current, and Pulse output.

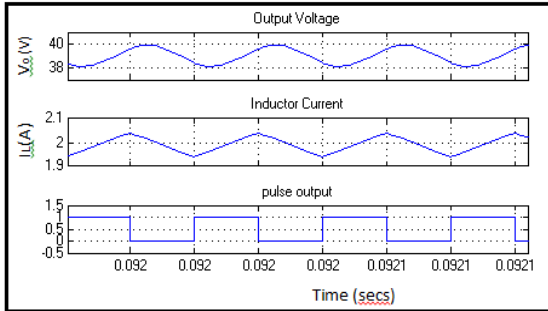


Fig. 5. Simulated Fundamental waveform when $I_{ref}=2.03A$.

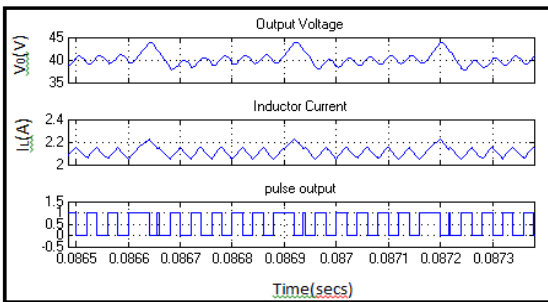


Fig. 6. Simulated Quasi periodic waveform when $I_{ref}=2.15A$.

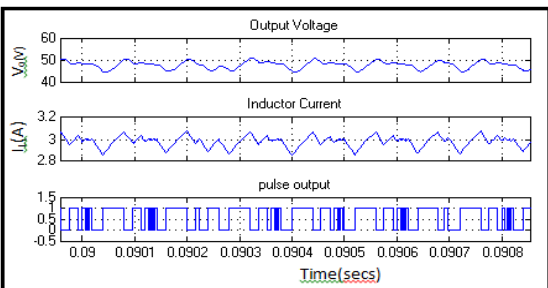


Fig. 7. Simulated Chaos waveform when $I_{ref}=3A$.

3.2. Derivation of Jacobian Matrix

To analyze the bifurcation behavior of the system, the Jacobian matrix is derived as follows and Eigen values are found to arrive at the boundary region between the stable and unstable mode of operation.

The state space averaged model is derived from the two state equations (1) and (2).

$$\begin{aligned} A_{eq} &= A_1(d) + A_2(1-d) \\ B_{eq} &= B_1(d) + B_2(1-d) \end{aligned} \tag{9}$$

Where A_1 and A_2 are the state matrix during ON and OFF condition of the switch. B_1 and B_2 are the input matrix during ON and OFF condition. The equivalent averaged state matrix A_{eq} is used to determine the stability state of the system by determining the eigen values.

$$A_{eq} = \begin{bmatrix} 0 & 0 & \frac{d}{C_1} & -\frac{1}{C_1} \\ 0 & \frac{1}{RC_2} & -\frac{1}{C_2} & \frac{1}{C_2} \\ \frac{d}{L_1} & -\frac{1}{L_1} & 0 & 0 \\ -\frac{1}{L_2} & \frac{1}{L_2} & 0 & 0 \end{bmatrix} \quad B_{eq} = \begin{bmatrix} 0 \\ 0 \\ \frac{1}{L_1} \\ 0 \end{bmatrix} \tag{10}$$

The switching function for current mode control is

$$s = i_{ref} - i_{L1} = 0 \tag{11}$$

$$\frac{d i_{L1}}{dt} = 0$$

From the state equation during ON condition, the equivalent value of duty ratio is derived based on the equation (10) and equation (11).

$$d_{eq} = \left[\frac{L_1(i_{ref} - i_{L1})}{V_{in} - V_{C_2} + V_{C_1}} \right] \tag{12}$$

The traditional analysis is used to locate the Eigen values for the transition of the state from stable to unstable region. The first step is to find the iterative function $f(.)$ and then to find the characteristics multipliers based on the equilibrium point. The four state variables from the state space averaged model are reduced into three iterative functions $f_1, f_2,$ and f_3 from the equations (10), (11), and (12).

$$f_1 = \left(\frac{d_{eq}}{C_1} \right) i_{L1} - \frac{i_{L2}}{C_1} \tag{13}$$

$$f_2 = \frac{V_{C2}}{RC_2} - \frac{i_{L1}}{C_2} + \frac{i_{L2}}{C_2} \tag{14}$$

$$f_3 = -\frac{V_{c1}}{L_2} + \frac{V_{C2}}{L_2} \tag{15}$$

The characteristics multipliers are the roots, λ , of the characteristics equation

$$\det(\lambda I - J_F(X)) = 0 \tag{16}$$

where $J_F(X)$ is the Jacobian matrix derived from the equivalent value of state variables based on the equations (12) to (15).

$J_F(X)$ is given by

$$J_F(X) = \begin{bmatrix} \frac{\partial f_1}{\partial V_{C_1}} & \frac{\partial f_1}{\partial V_{C_2}} & \frac{\partial f_1}{\partial i_{L_2}} \\ \frac{\partial f_2}{\partial V_{C_1}} & \frac{\partial f_2}{\partial V_{C_2}} & \frac{\partial f_2}{\partial i_{L_2}} \\ \frac{\partial f_3}{\partial V_{C_1}} & \frac{\partial f_3}{\partial V_{C_2}} & \frac{\partial f_3}{\partial i_{L_2}} \end{bmatrix} \quad (17)$$

The Eigen Values from the Jacobian matrix can be computed from the above equation using MATLAB coding. Table 2 shows the Eigen value movement of the Current mode controlled CIO boost converter based on the different values of the reference current. When the reference current is varied above 2.09A the real part of Eigen values moves from negative to positive, the system loses its stability and it enters into the chaotic region through quasi periodic bifurcation.

This theoretical analysis is used to find the stability region of the converter. When the AC power is given as input source, then it is very essential to get the voltage regulation using the outer voltage loop and the power factor correction in the input side of the converter using the inner current loop. Therefore, the converter can be implemented using the Average current mode controller and General pulse width modulation controller.

Table 2. Eigen Values From Jacobian Matrix.

Reference Current	Eigen Values	Remarks
2	-0.0062±j0.1908,-0.0356	STABLE
2.03	-0.0052±j0.1905,-0.0479	STABLE
2.09	-0.0024±j0.1854,-0.0521	STABLE
2.15	0.00034±j0.1749,-0.0577	UNSTABLE
2.5	0.00284±j0.1711,-0.0642	UNSTABLE
3	0.00154±j0.1623,-0.0895	UNSTABLE

4. PFC CONVERTER CIRCUIT WITH AVERAGE CURRENT MODE CONTROLLER

The circuit diagram of the PFC boost converter with the average current mode controller is shown in Fig.8. The input given to the converter is the rectified voltage from the diode bridge rectifier. When the output voltage (V_o) of the converter is compared with the reference voltage (V_{ref}), the error signal is fed to the PI controller to derive the control signal. The output of the PI controller is multiplied with the scaled replica of rectified line voltage to get the reference current, which is $i_{ref}(t) = I_e \sin(\omega t)$ where ω is the angular frequency of the line signal and I_e is the maximum amplitude.

To turn ON the switch the set-reset (SR) flip-flop (FF) is set periodically by the clock signal. The reference current is compared with the input inductor current. When it reaches the sinusoidal reference, the output of the comparator resets the flip-flop, thereby turning off the switch. The cycle repeats when the flip-flop is set again by the clock signal. When the reference voltage is changed significantly the current $i_{ref}(t)$ is

also changed. Hence, the average current controller makes the average input current to be proportional to the input voltage. Therefore, the input current is made to follow with reference current to attain a unity power factor. (Herbert, H.C., 2003).

The phase waveform of the input voltage (scaled down) and input current are shown in Fig.9 and Fig.10. The power factor correction converter operated with the designed load resistance of 40Ω, during which it can be observed that there is a distortion in the current waveform for the ACM controller.

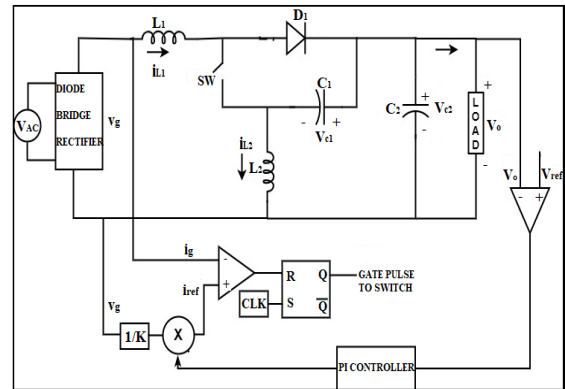


Fig. 8. Circuit diagram for PFC converter with ACM controller.

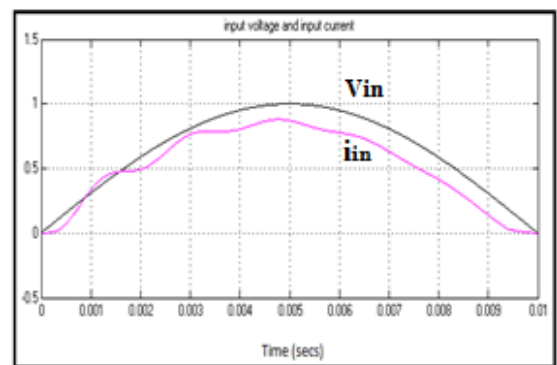


Fig. 9. Simulated waveform for input voltage and input current with ACM controller.

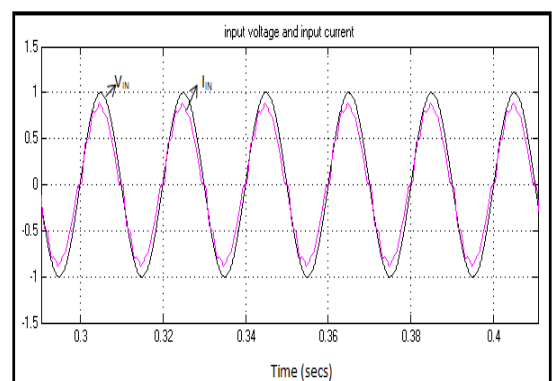


Fig. 10. Simulated waveform for unity power factor with ACM controller.

5. PFC CONVERTER CIRCUIT WITH GPWM CONTROLLER

To overcome the problem, persist in the ACM controller, the GPWM controller is applied to get the unity power factor with reduced input distortion. The circuit diagram for the PFC converter with the GPWM controller is shown in Fig.11. A single-phase diode bridge followed by a dc-dc converter with proper control forms a rectifier with active power-factor correction (PFC).

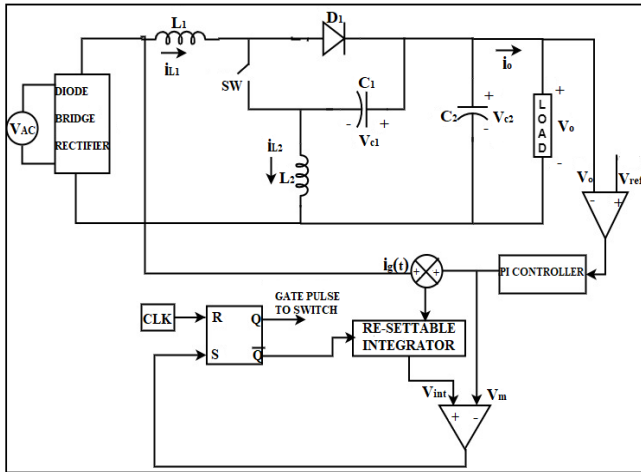


Fig. 11. Circuit Diagram for PFC converter with GPWM controller.

When the controller forces the input current to have the same shape as the input voltage so that the input impedance appears to be resistive, that rectifier is called as resistor emulator. The resistor emulator not only requires a near-unity power factor but also has low harmonic content in the line current. There are two traditional approaches to control a resistor emulator, namely, the voltage follower approach and the multiplier approach (Zheren Lai., 1998). In the GPWM control method, the voltage follower approach is applied to get the improved current waveform with a unity power factor for both load and line variation.

The components for a general pulse width modulation technique are (i) constant-frequency clock generator,(ii)flip flop (FF),(iii)comparator (CMP),(iv) Resettable integrator. The voltage controller compares the actual voltage with the reference and the error signal is added with the product of input current (i_{in}) and sensing resistance R_s that is $i_g(t)$. This is fed as the input to the GPWM controller. The clock generator is used to initiate the Flip Flop with fixed switching frequency (f_s) to turn ON the switch used in the converter and to turn OFF the integrator switch. The integral time constant is equal to the constant switching period T_s . The output Q of the Flip flop goes to a high state if the resettable integrator performs the normal integral operation.

The integrator output voltage V_{int} is compared with the modulation voltage V_m . When the integrator output voltage is equal to modulation voltage ($V_{int} = V_m$), the comparator output is used to reset the converter switch S and integrator switch simultaneously. The switch S is then turned off. Again the

next cycle repeats when the Flip flop is initiated by clock generator with a constant frequency.

5.1 The control law

$$InputCurrent\ i_g = \frac{v_g}{R_e} \tag{18}$$

Where R_e is the emulated resistance

The input current i_g is controlled by modulating the duty ratio d .

$$i_g R_s = \frac{V_m}{M(d)} \tag{19}$$

Where R_s is the equivalent current sensing resistance

V_m is the modulation voltage from the voltage controller.

$M(d)$ is the voltage conversion ratio of the dc to dc converter.

$$M(d) = \frac{1}{1-d} \tag{20}$$

To get unity power factor, the input current should follow the inductor current of the converter. It can be represented as $i_g = i_{in} = i_{L1}$.

$$R_s(i_{in}) = \frac{V_m}{1-d} \tag{21}$$

$$R_s(i_{in}) = V_m(1-d)$$

$$Output\ Voltage\ V_o = \frac{V_{in}}{1-d} \tag{22}$$

From the above equations the inductor current is derived as

$$i_{L1} = \frac{V_m * V_{in}}{V_o R_s} \tag{23}$$

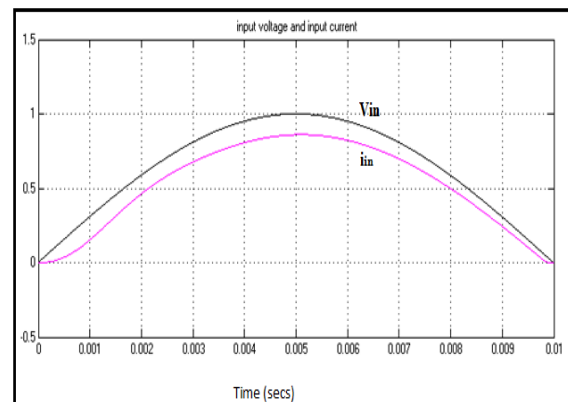


Fig. 12. Simulated waveform for input voltage and input current for GPWM controller.

When it follows the input voltage and input current of the rectifier, the unity power factor is achieved with reduced input distortion (Zheren Lai., 1998). The unity power factor waveform for the GPWM controller with scaled down input voltage and input current is shown in Fig.12 and Fig.13. It shows that the shape of the input current is improved in the GPWM controller with reduced distortion.

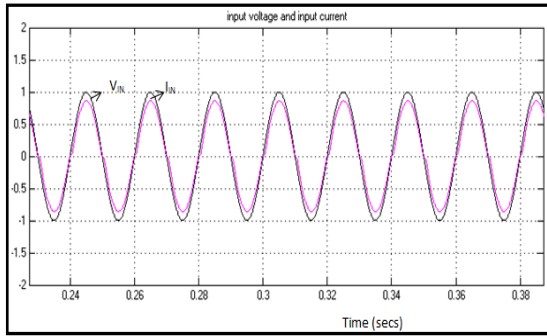


Fig. 13. Simulated Waveform for Unity power factor with GPWM controller.

5.2 Comparative Analysis

Line variation: The input voltage is varied from 20V to 100V and it is plotted with total harmonic distortion (THD). The THD value is nearly 5% in the GPWM controller at 100V input source compared to the ACM controller. The power factor is nearly unity in the GPWM controller as shown in Fig.14 and Fig.15.

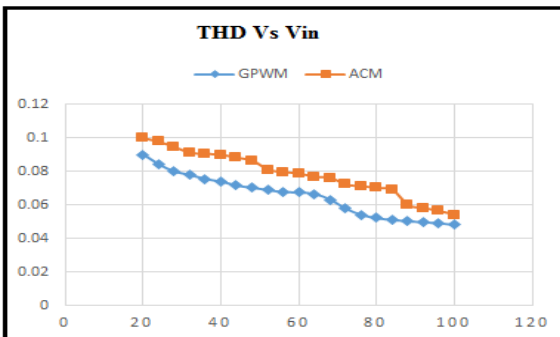


Fig. 14. THD Vs input voltage for GPWM and ACM controllers.

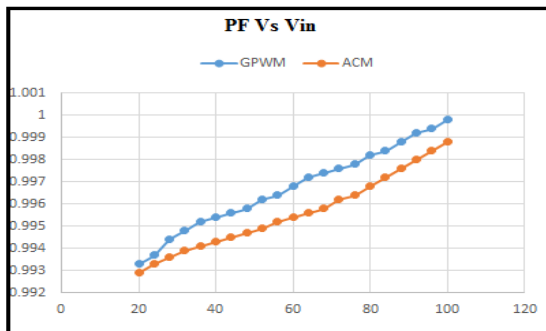


Fig. 15. PF Vs Input voltage for GPWM and ACM controllers.

Load Variation: When the load resistance is varied from 25Ω to 100Ω, the total harmonic distortion (THD) value is low in the GPWM controller when compared to the ACM controller and the power factor is improved for the GPWM controller as shown in Fig.16 and Fig. 17. In the FFT analysis, the THD value is 7.42% under the ACM controller and it is 6.01% under the GPWM controller for the designed load resistance as shown in Fig. 18 and Fig. 19.

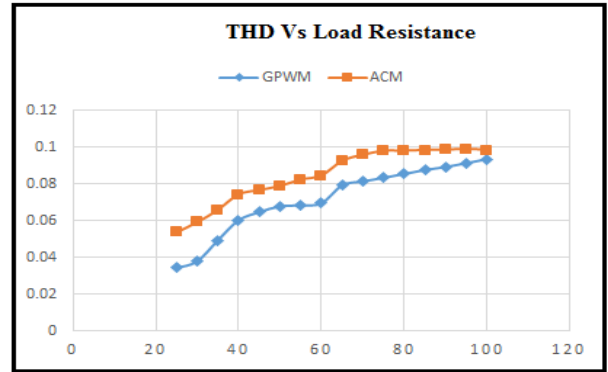


Fig. 16. THD Vs Load resistance for GPWM and ACM controllers.

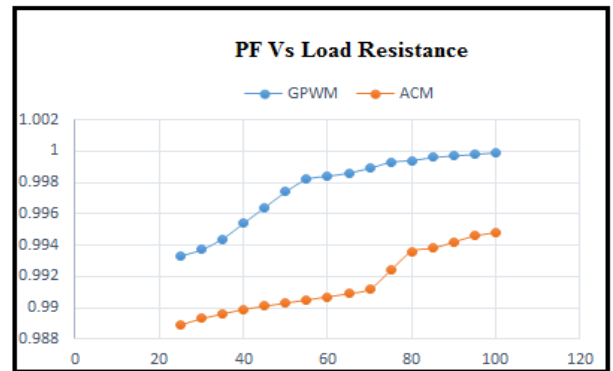


Fig. 17. PF Vs Load resistance for GPWM and ACM controllers.

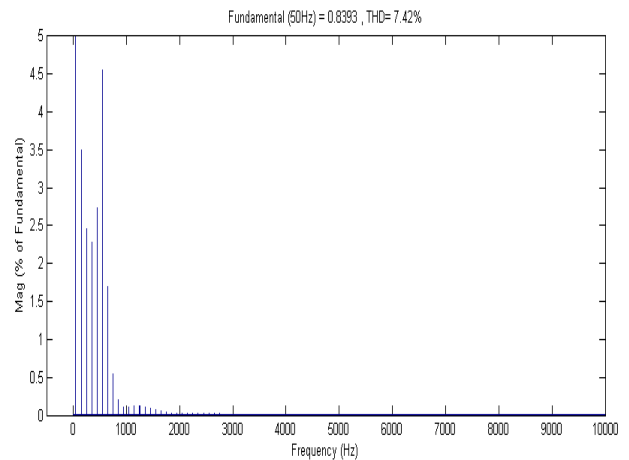


Fig. 18. FFT analysis for ACM controller.

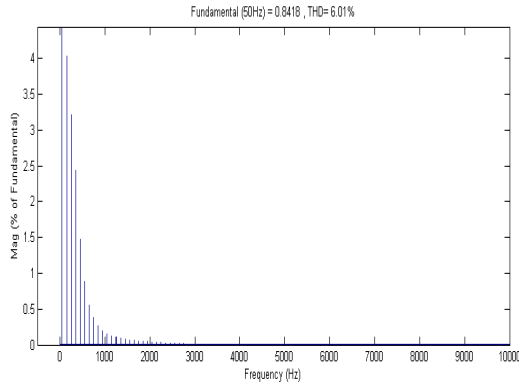


Fig. 19. FFT Analysis for GPWM controller.

6. EXPERIMENTAL RESULTS

The hardware implementation of the converter is realized for ACM and GPWM active PFC controllers. A 230 V, 50 Hz power supply is stepped down and then it is given to the diode bridge rectifier. The rectified input voltage is fed to the input of the Continuous input and output power Boost converter. The switch used in the converter circuit is MOSFET IRF540. The control circuit is implemented using an IC PIC 16F877A. The experimental pulse generated with duty ratio 0.5 is shown in Fig.20.

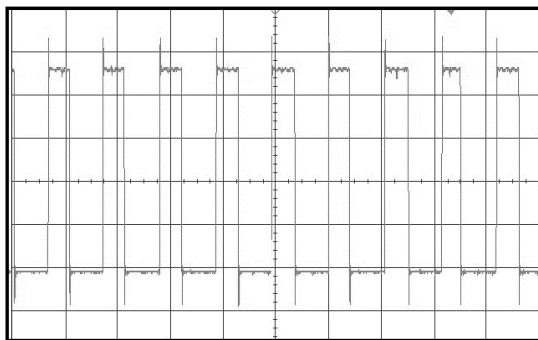


Fig. 20. Experimental Pulse Generated given to the Switch.

The experimental steady state output current is shown in Fig.21. The experimental fundamental output voltage and the inductor current waveform for the reference current 2.03A are shown in Fig.22. When the reference current is further increased the converter operation moves into the chaotic region through quasi periodic bifurcation are shown in Fig.23 and Fig.24.

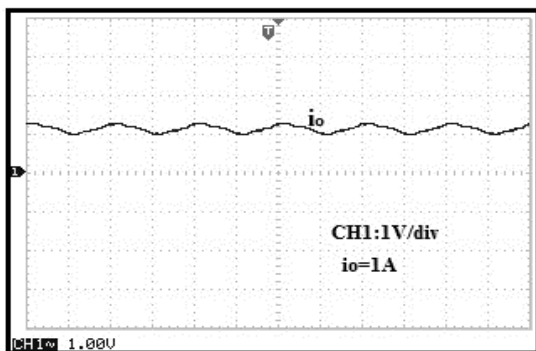


Fig. 21. Experimental Output Current Waveform.

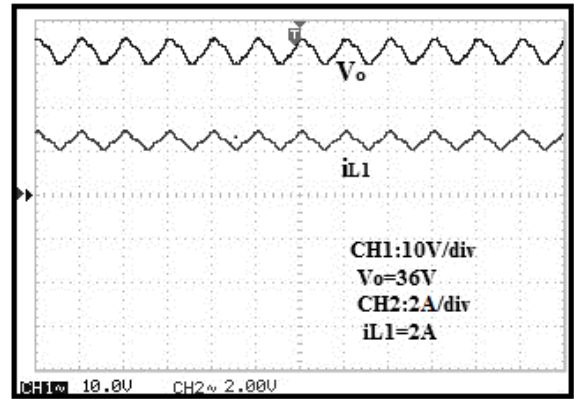


Fig. 22. Experimental Fundamental Output Voltage and Inductor Current.

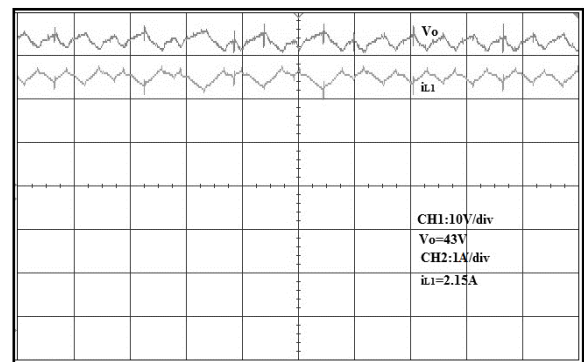


Fig. 23. Experimental Quasi periodic Output Voltage and Inductor Current.

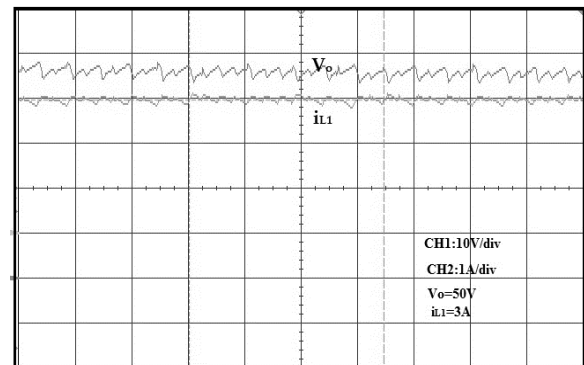


Fig. 24. Experimental Chaotic Output Voltage and Inductor Current.

The IC PIC 16F877A is coded to work under two modes of operation by using the mode changing switches, to perform both the ACM and GPWM controllers. Fig.25 shows the experimental waveform results with the input voltage and input current in phase. It is evident that the displacement factor is unity i.e., the input voltage and current waveforms in the ACM controller are in phase, but they show distortions.

It is found that the GPWM controller exhibits better control in Continuous input and output power Boost PFC converter with reduced distortions. The input current waveform is improved and the unity power factor is achieved in the

GPWM controller compared to the ACM controller as shown in Fig.26.

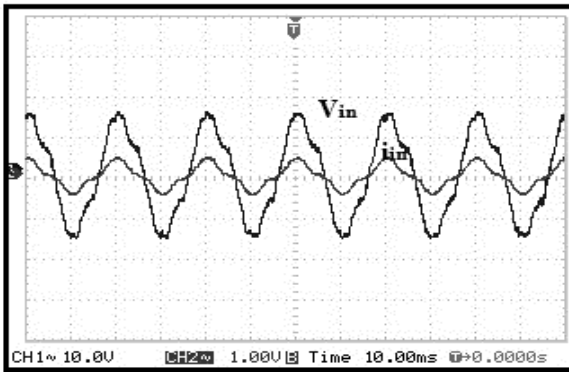


Fig. 25. Unity Power Factor waveform for ACM controller.

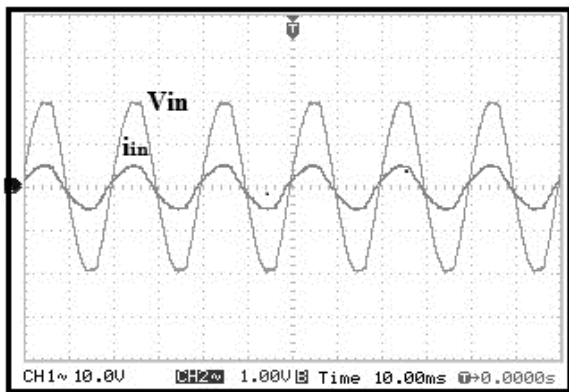


Fig. 26. Unity Power Factor waveform for GPWM Controller.

7. CONCLUSION

The stability of the Continuous input and output power boost converter was analyzed to get the stable operating region of the converter under the variation of the reference current. Theoretical analysis of current mode control shows the movement of Eigen values found using the Jacobian matrix. When the converter was implemented with the ACM controller the FFT analysis shows the 7.42% THD with the designed load resistance value. It is reduced into 6.01% with the GPWM controller. The power factor is achieved into nearly unity value with load and line variation and the shape of the input current waveform is also improved. The comparative analysis, simulation, and experimental results show that the proposed GPWM controller achieves the unity power factor for Continuous input and output power boost converter.

REFERENCES

Aroudi, El., Orabi, M., Martínez-Salamero, L.(2008). A representative discrete-time model for uncovering slow and fast scale instabilities in boost power factor correction AC-DC pre-regulators, *International Journal of Bifurcation and Chaos*, 18(10), pp.3073-3092.

Bhim, Singh., Radha, Kushwaha.(2019).EV battery charger

with non-inverting output voltage-based bridgeless PFC Cuk converter, *IET Power Electronics*,12(13),pp. 3359 – 3368.

Chu,G.,Tse,C.K.,Wong,S.C.(2009).Line-frequency instability of PFC power supplies, *IEEE Transactions on Power Electronics*,24(2), pp.469-482.

Deivasundari,Parvathyshankar.,Uma,Govindarajan.,Uma MaheswariMallapu,Gopinath.,Kavitha,Anbukumar.(2013).Coexistence of fast-scale and slow-scale instability in CUK power factor correction AC-DC pre-regulators under non-linear current-mode control, *IET Power Electronics*,6(1),pp.78-87.

Faqiang, Wang., Hao,Zhang., Xikui, Ma. (2010). Analysis of slow-scale instability in boost PFC converter using the method of harmonic balance and Floquet theory, *IEEE Trans. Circuits Syst. I*, 57(2), pp.405-414.

Giaouris,D.,Banerjee,S.,Zahawi,B.,Pickert,V.(2007).Control of fast scale bifurcations in power factor correction converters, *IEEE Transactions on Circuits and Systems*,54, pp.805-809.

H.H.C,lu.,Tse,C.K.(2003).Study of low-frequency bifurcation phenomena of a parallel connected boost converter via simple averaged models, *IEEE Transactions on Circuits and Systems*.50, pp.679-686.

Hao,Zhang., Yuan,Zhang.,Xikui,Ma.(2012). Distortion Behavior Analysis of General Pulse-Width Modulated Zeta PFC Converter Operating in Continuous Conduction Mode, *IEEE Transactions On Power Electronics*,27(10), pp. (4212-4223).

Hengsi, Qin., Jonathan Kimball,W.(2011).Generalized Average Modeling of Dual Active Bridge DC-DC Converter, *IEEE Transactions on Power Electronics*,27(4),pp.2078-2084.

Herbert, H.C., Zhou, Y., Tse, C.K. (2003).Fast scale instability in a PFC boost converter under average current mode control, *Int. Journal of Circuit Theory and Appl.*,31, pp. 611-624.

Hu, W., Zhang, B., Yang, R., Qiu, D.(2017).Dynamic behaviours of constant on-time one-cycle controlled boost converter, *IET Power Electronics*. 11(1), 160-167.

Kavitha, A., Uma,G.(2010).Resonant Parametric Perturbation Method to Control Chaos in Current Mode Controlled DC-DC Buck-Boost Converter, *Journal of Electrical Engineering & Technology*,5(1), pp. 171-178.

Kavitha,A.,Uma,G.,BeniReesha,M.(2012). Analysis of fast-scale instability in a power factor correction Cuk converter, *IET Power Electronics*, 5,pp.1333-1340.

Maheswari,E.,Kavitha,A.(2016).Bifurcation Analysis in Continuous Input Output Buck Boost PFC Converter, *International Conference on Computation of Power, Energy Information and Communication (ICCPEIC)*,IEEE, pp 490-495.

Masoud,Bahmanpour., Hamid Reza, Koofigar., Majid, Delshad., Mohammad, Hasan Tosifian.(2019).Nonlinear Control and Implementation of a Hybrid Power System, *Journal of control engineering and applied informatics*, 21(1), pp.70-78.

Mazumder, S.K., Nayfeh, A.H., Boroyevich,D.(2001). Theoretical and experimental investigation of the fast-

- and slow-scale instabilities of a DC–DC converter, *IEEE Trans. Power Electron.*,16(2), pp 201–216.
- Mei,Su., Zhangjie,Liu.,Yao,Sun., Hua,Han., Xiaochao,Hou. (2016). Stability Analysis and Stabilization Methods of DC Microgrid With Multiple Parallel-Connected DC–DC Converters Loaded by CPLs, *IEEE Transactions on Smart Grid*,9(1),pp.132-142.
- Muamer, M. Shebani.,Tariq Iqbal,M.,John, E. Quaicoe. (2020). Control Algorithm for Equal Current Sharing between Parallel-Connected Boost Converters in a DC Microgrid, *Hindawi, Journal of Electrical and Computer Engineering*, Volume 2020,pages11.<https://doi.org/10.1155/2020/6876317>.
- Nahla,E.Zakzouk.,Ahmed,K.Khamis,Ahmed,K. Abdelsalam.,Barry,W.Williams.(2019).Continuous-Input Continuous-Output Current Buck-Boost DC/DC Converters for Renewable Energy Applications: Modelling and Performance Assessment, *Energies*, 12(11), 2208; doi:10.3390/en12112208
- Orabi,M.,Ninomiya,T.(2003).Nonlinear dynamics of power-factor-correction converter, *IEEE Transactions on Industrial Electronics*, 50(6), pp. 1116–1125.
- Radha,Munuswamy.,Uma,Govindarajan., Kavitha,Anbukumar.(2020).Performance comparison and stability analysis of ACM and ENLC controlled SEPIC PFC converter, *IET Power Electronics*, 13(5), pp.991-1001.
- Ruiye,Zhang.,Aiguo,Wu.,Zenghui,Wang.,Shijian,Cang. (2019).Chaotic and sub harmonic oscillations in a DC–DC boost converter with PWM voltage–current hybrid controller and parallel MR load, *Non linearDynamics, Springer*,<https://doi.org/10.1007/s11071-019-05357-z>.
- Sajid,Iqbal., Xizhe,Zang., Yanhe, Zhu., Jie, Zhao.(2014). Study of bifurcation and chaos in DC-DC boost converter using discrete-time map, *International IEEE Conferenec*,3-5 July 2014.
- Tse,C.K.(2003). Complex Behaviour of Switching Power Converters, Boca Raton, FL: CRC PRESS.
- Wei,Ma.,Mingyu,Wang.,Shuxi,Liu.,Shan,Li.,Peng,Yu. (2011). Stabilizing the Average Current Mode Controlled Boost PFC Converter via Washout Filter Aided Method, *IEEE Transactions on Circuits and Systems*,58, pp.595-599.
- Weibin,C.,Jiuxu,S.,Hong,Li.,Yingna,G.(2015).Time Varying compensation for Peak Current Controlled PFC Boost converters, *IEEE Transactions on Power Electronics*,30,pp.3431-3437.
- Williams,B.W.(2013).DC-to-DC Converters with Continuous Input and Output Power, *IEEE Power Electronics Society*,28(5),pp.2307-2316.
- Xiang, Lin.,Faqiang,Wang.,Herbert, H. C. lu.(2018). A New Bridgeless High Step-up Voltage Gain PFC Converter with Reduced Conduction Losses and Low Voltage Stress,*Energies*,11(10),2640,<https://doi.org/10.3390/en11102640>.
- Xiaotian, Zhang., Joseph,W. Spencer.(2011). Analysis of Boost PFC Converters Operating in the Discontinuous Conduction Mode, *IEEE Transactions on Power Electronics*, 26(12),pp.3631-3628.
- Yang-Lin,Chen.,Yaow-Ming,Chen.(2016).Line Current Distortion Compensation for DCM/CRM Boost PFC Converters, *IEEE Transactions on Power Electronics*,31(3),pp.2026-2038.
- Yesodha,V.,Kavipriya,R., Joshna,T.S.,Rajini,V.(2013). Analysis of Chaos and Bifurcation in DC-DC Converters Using MATLAB, *ICCPCT, IEEE Conference*. Doi:10.1109/ICCPCT.2013.6528911.
- Yi-Hung Liao.(2020).A Step up/down Power Factor correction Converter with modified Dual Loop Control,*Energies*,13(1),199,<https://doi.org/10.3390/en13010199>.
- Zheren, Lai., Keyue, Ma Smedley.(1998). A Family of Continuous-Conduction- Mode Power-Factor-Correction Controllers Based on the General Pulse-Width Modulator, *IEEE Transactions On Power Electronics*,13(3),pp.501-510.
- Zhioua, M.,Aroudi,A.El.,Belghith,S.,Bosque Moncusi,J.M., Giral,R.,Al-Hosani,K.,Al-Numay.M.(2016).Modeling, Dynamics, Bifurcation Behavior and Stability Analysis of a DC–DC Boost Converter in Photovoltaic Systems, *International journal of Bifurcation and Chaos*,26(10), pp.1650166-1-16.
- Zhuang, Fusheng ., Naayagi.R.T.(2018).Power Converters for DC Microgrids – Modelling and Simulation, *IEEE Innovative Smart Grid Technologies - Asia (ISGT Asia)*, DOI: 10.1109/ISGT-Asia.2018.8467847.